Research Square

Preprints are preliminary reports that have not undergone peer review.
They should not be considered conclusive, used to inform clinical practice,
or referenced by the media as validated information.

Aluminum exposure impairs the reproductive function of male mice by inhibiting the AKAP4/cAMP/PKA signaling pathway and inducing mitochondrial apoptosis

Hongfei Hu
The Affiliated Hospital of Youjiang Medical University for Nationalities
Guangji Wei
Baise People's Hospital
Hai Lan
Graduate School of Youjiang Medical University for Nationalities
Ningsiwei Chen
Hebei North College
Yang Feng
Graduate School of Youjiang Medical University for Nationalities
Huixin Peng
The second people's hospital of jinzhong
Zhenying Yang
Graduate School of Youjiang Medical University for Nationalities
Yanxin Huang
The Affiliated Hospital of Youjiang Medical University for Nationalities
Shihua Luo
The Affiliated Hospital of Youjiang Medical University for Nationalities
Wencheng Chen
chwch3268@sina.com

The Affiliated Hospital of Youjiang Medical University for Nationalities

Research Article

Keywords: Aluminum exposure, mitochondrial damage, PKA signaling pathway, phosphorylation, apoptosis, male reproductive toxicity

Posted Date: April 6th, 2026

DOI: https://doi.org/10.21203/rs.3.rs-9115975/v1

License: This work is licensed under a Creative Commons Attribution 4.0 International License.
Read Full License

Additional Declarations: No competing interests reported.

Abstract

Aluminum (Al), a widely distributed environmental heavy metal, has attracted growing attention for its reproductive toxicity. The present study aimed to examine the toxicological impact of $AlCl_3$ on the male reproductive system and delineate its molecular basis, with emphasis on the involvement of the AKAP4-regulated cAMP/PKA signaling pathway in mitochondrial function and apoptosis. Using an $AlCl_3$-exposed mouse model and GC-2spd cells, together with Western blotting, immunofluorescence, and mitochondrial functional assays, Al accumulation in testicular tissue was observed, accompanied by pathological injury, reduced sex hormone levels, and abnormal sperm parameters. Mechanistic analysis in vitro demonstrated marked suppression of AKAP4 expression in GC-2spd cells following $AlCl_3$ treatment, resulting in diminished cAMP/PKA activity. The consequent reduction in p-BADSer155 phosphorylation, coupled with elevated BAD expression, triggered mitochondrial dysfunction—evidenced by decrease in ATP production and reduced membrane potential—and initiated apoptosis, characterized by Bax/Bcl-2 disequilibrium, Cytochrome C release, and caspase-3 activation. Gene editing further confirmed that AKAP4 overexpression alleviated $AlCl_3$-induced inhibition of the cAMP/PKA pathway, mitochondrial dysfunction, and apoptosis in GC-2spd cells. Collectively, these results identify the AKAP4–cAMP/PKA–BAD phosphorylation axis as a core mediator of Al-induced reproductive toxicity, offering mechanistic insight into male infertility associated with heavy metal exposure and indicating AKAP4 as a potential therapeutic target.

1 Introduction

Aluminum (Al), one of the most abundant elements in the earth's crust, is extensively applied in daily life, industrial production, and healthcare products owing to its favorable metallic properties and low production cost. However, the discharge of Al-containing waste and wastewater has generated severe environmental hazards[1]. In addition, Al compounds are widely incorporated into unavoidable products such as drinking water treatment agents, food additives, antiperspirants, and vaccine adjuvants, leading to continuous exposure of humans and animals through water, food, pharmaceuticals, and the environment, thereby imposing substantial risks to health and survival[2]. Evidence indicates that Al enters the human body via multiple routes, including ingestion, inhalation, and medication, and due to its extended half-life of 3.5–8 years[3, 4], elimination from the body remains inefficient. This persistence results in long-term bioaccumulation and subsequent toxicity. Chronic exposure has been linked to neurodegenerative disorders such as Parkinson's disease and Alzheimer's disease, establishing Al as a recognized neurotoxin[5]. Furthermore, increasing reports highlight its detrimental impact on the urinary system[1], locomotor system[6], cardiovascular system[7], digestive system[2, 8], and reproductive system[9–11]. Collectively, the toxicological significance of Al necessitates heightened scientific scrutiny and systematic investigation.

Globally, infertility affects approximately 8–12% of couples[12], ranking as the third most persistent disease burden after cancer and cardiovascular disorders, and has emerged as a major public health challenge. Epidemiological investigations indicate that nearly 85% of infertile couples have identifiable

etiologies, with male factors contributing to roughly half of the cases[13]. Alarmingly, male sperm quality has shown a sustained decline over recent decades, with total sperm counts reduced by nearly 60%[14]. Multiple determinants account for the deterioration in sperm quality and quantity, among which environmental pollution has drawn increasing attention due to its recognized impact on reproductive health. Al, a prevalent metal contaminant, has repeatedly been shown to impair male reproductive potential. Evidence from prior studies demonstrates that exposure of human sperm to Al, Cd, or Pb markedly reduces motility, with Al exerting the most severe impairment[15]. In a semen survey involving 62 patients, the mean Al concentration reached 339 μg/L, with a maximum level of 1547.8 μg/L, markedly exceeding the values observed in normal human semen[16]. Extensive animal experiments further corroborate this observation. In male rats, 60 days of dietary Al exposure at human-equivalent levels impaired testicular function by inducing oxidative stress through elevated ROS and MDA, suppressing spermatogenesis, and reducing reproductive capacity[17]. Agata et al. demonstrated that Al accumulated in the testicular tissue of Bank Voles, leading to diminished fertility[18]. Consistent evidence from in vitro studies confirmed that Al exposure damaged the activity of spermatogenic cells in rabbits and mice[19]. Although current data establish that Al can accumulate in testicular tissue, disrupt the blood-testis barrier, and consequently impair sperm quality and fertility, existing research has largely concentrated on oxidative stress and necrotic injury. The precise molecular mechanisms underlying Al interference with spermatogenesis remain unresolved, particularly the specific alterations in mitochondrial function and apoptosis-regulatory pathways, which have yet to be systematically delineated.

Spermatogenesis relies heavily on both cellular energy metabolism and modulation of apoptosis. Mitochondria, functioning as the primary energy producers and executors of apoptotic signaling, critically determine the survival and differentiation of spermatogenic cells[20]. Evidence indicates that cAMP-dependent protein kinase A (PKA) serves as an essential regulator of mitochondrial function in testicular cells[21]. PKA phosphorylates the pro-apoptotic protein BCL-2 Associated Death Promoter (BAD) at Ser155, preventing its binding to the anti-apoptotic protein BCL-2 and thereby suppressing mitochondrial apoptotic signaling[22, 23]. The localization and function of PKA are determined by the spatiotemporal regulation of A-kinase anchoring proteins (AKAPs). Among them, AKAP4, a testis-specific anchoring protein, positions PKA at the sperm flagellum and mitochondrial sheath, directly influencing sperm motility and mitochondrial performance[24, 25]. Increasing evidence suggests that environmental stressors can alter AKAP expression; for instance, fluoride exposure impairs sperm quality by reducing AKAP4 expression in male mouse testes[26]. Consistent with this, our proteomic analyses revealed significant downregulation of AKAP4 in rat testes following Al exposure[27]. Database-based interaction analysis further demonstrated that AKAP4 associated with both regulatory subunits of PKA (Fig. 3a). Despite these observations, it remains unclear whether Al interferes with the AKAP4-mediated cAMP/PKA signaling axis. Accordingly, the central hypothesis of this study proposes that Al diminishes AKAP4 expression, impairs PKA-dependent phosphorylation of BAD, disrupts mitochondrial function, and consequently induces spermatogenic cell apoptosis leading to male reproductive toxicity.

2 Materials and Methods

2.1 Main Reagents

$AlCl_3$ hexahydrate ($AlCl_3$·6H2O, L1706080) was obtained from Aladdin Biochemical Technology Co., Ltd. (Shanghai, China). ATP (S0026) and BCA protein (P0009) assay kits were acquired from Beyotime (Shanghai, China). The cyclic adenosine monophosphate (cAMP) assay kit was purchased from Jianglai Biotech (Shanghai, China). Mitochondrial Membrane Potential Assay Kit (with JC-1, E-CK-A301) and the TUNEL staining kit (E-CK-A325) was obtained from Elabscience. CCK8 (CT0001-B) was supplied by Sparkjade (Shandong, China). A-Kinase Anchoring Protein 4 (AKAP4, PA5-109377) and BCL2-associated agonist of cell death (BAD, MA5-31978) were purchased from Thermo Fisher Scientific (Massachusetts, USA). Protein Kinase A (PKA, 861081), B-cell lymphoma 2 (Bcl-2, 381702), Cytochrome C (Cyt C, R22867) Bcl-2-associated X protein (Bax, R380709), and housekeeping gene GAPDH (R380626) antibody and horseradish peroxidase (HRP)-conjugated secondary antibodies were acquired from Zen-Bioscience (Chengdu, China). Phosphorylated BAD (p-BADSer155, CST-9297) and cleaved caspase-3 (CC3, CST-9661) were purchased from Cell Signaling Technology (Massachusetts, USA).

2.2 Animals and Treatment

Thirty-two male C57BL/6J mice (4–6 weeks old, 20–25 g) were obtained from Charles River Laboratory Animal Technology Co., Ltd. (Guangdong, China) and randomly allocated into four groups (n = 8 per group). After one week of dietary adaptation, the animals were housed under standard conditions (maximum four per cage, 24–27°C, 50%–70% relative humidity, 12-h light/dark cycle). The Agency for Toxic Substances and Disease Registry (ATSDR) has established a chronic oral minimal risk level (MRL) of 1 mg Al/kg·day for healthy human populations. To adapt this value for experimental purposes, an interspecies scaling approach based on the no-observed-adverse-effect level (NOAEL) was employed. The equivalent murine dose was calculated as follows: Murine dose = 1 mg/(kg·day) × 1/0.0811 ≈ 12.35 mg/(kg·day), where the factor 0.0811 represents the human-to-mouse body surface area conversion coefficient recommended by the Food and Drug Administration (FDA). This scaled dose was subsequently integrated with our previously established aluminum exposure model, thereby providing a robust foundational framework for the experimental design[28]. In the study, mice received intraperitoneal $AlCl_3$ injections for 9 weeks, five times per week, at doses corresponding to the control (C, 0 mg/kg/d), low (L, 5 mg/kg/d), medium (M, 10 mg/kg/d), and high (H, 20 mg/kg/d) groups (see Fig. 1a for the experimental scheme). At the end of the exposure period, mice were anesthetized with 200 mg/kg pentobarbital before surgery. Blood was collected via orbital sampling, and serum was separated by centrifugation. The epididymis was immediately excised and incubated in PBS at 37°C for sperm analysis. Testes were weighed, fixed in 4% paraformaldehyde, and stored at − 80°C together with serum for subsequent assays. All procedures strictly complied with the *Guide for the Care and Use of Laboratory Animals* and were approved by the Ethics Committee of Youjiang Medical University for Nationalities.

2.3 Testicular Al Content

Al content in testicular tissue was quantified by inductively coupled plasma atomic emission spectrometry (ICP-AES). Briefly, 50 mg of tissue from each group was placed in a suitable vessel, treated with 5.0 mL of nitric acid, and evaporated at low temperature. Subsequently, 1.0 mL of perchloric acid was introduced until white fumes were released and a clear, colorless solution was obtained. The residue was transferred to a 10 mL volumetric flask and diluted to yield a 10% HCl solution. To verify measurement reliability, three blanks were included. The detection limit for Al was 9.5 μg/L, and data were expressed as mg/kg. Quantification was carried out under standardized ICP-AES operating conditions.

2.4 Hematoxylin and Eosin (H&E) Staining

Mouse testes were fixed in 4% paraformaldehyde for 12 h, dehydrated using a tissue dehydrator, embedded in paraffin, and sectioned at 4 μm thickness with a microtome. The sections underwent H&E staining and were subsequently examined and imaged under a light microscope.

2.5 Sperm Parameter Assessment

Following anesthesia, testes were excised and the epididymis carefully dissected. After transfer to a clean bench, the surrounding adipose tissue was removed, and the epididymal tissue was finely minced before being placed in a 2 ml centrifuge tube. The sample was incubated in HTF at 37°C for 10 min with continuous gentle agitation to ensure uniform release of sperm, generating a fresh suspension. A 10 μL aliquot was subsequently analyzed using the Computer-Assisted Semen Analysis (CASA) system (SSA-II, Gold Edition, Suijia Software, Beijing, China) in accordance with the WHO laboratory manual for sperm concentration and motility (6th edition). Quantitative assessment included sperm count, overall motility, and distribution of progressively motile (PR), non-progressive (NP), and immotile (IM) subpopulations.

2.6 Serum Hormone Levels

Serum testosterone (T), luteinizing hormone (LH), and follicle-stimulating hormone (FSH) concentrations were quantified using ELISA kits (Elabscience Biotechnology Co., Ltd.), with all experimental procedures conducted strictly following the manufacturer's protocols.

2.7 Immunohistochemical Staining

Paraffin-embedded tissue sections were dewaxed, rehydrated, and subjected to antigen retrieval in citrate buffer by pressure cooking at 140°C for 2 min 40 s, followed by natural cooling. Endogenous peroxidase activity was blocked by incubation with 3% H_2O_2 for 10 min at room temperature in the dark. After three washes with PBS, the sections were blocked with goat serum for 30 min. Primary antibodies against AKAP4, and PKA (1:300) were applied and incubated overnight at 4°C. The following day, after removal of the primary antibodies and PBS washing, HRP-conjugated secondary antibodies were applied and incubated at 37°C for 30 min. Subsequent PBS washes were followed by visualization with DAB solution until brown signals were observed microscopically. Nuclei were counterstained with hematoxylin for 1 min and differentiated with water for 15 min. Finally, the sections were mounted with resin and examined under a light microscope for imaging.

2.8 Cell Culture and Treatment

GC-2spd cells (CL-0593), immortalized spermatogonia derived from 6-week-old mice, were obtained from Wuhan Procell Life Science Co., Ltd. Cells were maintained in DMEM(H) (Gibco) supplemented with 10% fetal bovine serum (VivaCell, Shanghai, China) and 1% penicillin-streptomycin at 37°C in a 5% CO_2 incubator. An Al exposure gradient was established by treating cells with 0, 0.5, 1, 2, 4, 6, 8, or 10 mM $AlCl_3$ for 24 h. The concentration yielding cell viability above 75% was selected to ensure reliability in subsequent analyses. In addition, AKAP4 overexpression GC-2spd models were generated using complete sequence plasmid of CDS (Coding Sequence) obtained from GenePharma (Suzhou, China). All cultures were maintained under identical incubation conditions.

2.9 Cell Viability Assay

GC-2spd cells were seeded into 96-well plates at a density of 5×10^3 cells per well. Following attachment, cells were exposed to 2 mM $AlCl_3$ for 24 h. The medium was subsequently removed, and 10 μL of CCK-8 reagent was added to each well, followed by incubation at 37°C for 2 h. Absorbance at 450 nm was then recorded with a microplate reader. Blank wells without cells and untreated cell controls were included. Cell viability was calculated as: Cell viability (%) = (OD of experimental group – OD of blank group) / (OD of control group – OD of blank group) × 100%.

2.10 RNA Sequencing (RNA-seq) and Transcriptomic Analysis

GC-2spd cells were cultured to 75% confluence and treated with medium containing either 0 mM (control) or 2 mM $AlCl_3$ for 24 h. After exposure, cells were washed twice with PBS, and total RNA was extracted. RNA purity was verified by full-spectrum spectrophotometry using the A260/A280 ratio. Qualified samples were submitted to Shanghai Weihuan for sequencing. Transcript reconstruction was performed using StringTie based on HISAT2 alignments, and expression levels were quantified by TPM from raw read counts. Differentially expressed genes (DEGs) were defined by pvalue < 0.05 and $|\log_2FC| > 0.5$. Functional enrichment of selected DEGs was conducted through the GO (http://www.geneontology.org/) and KEGG (https://www.kegg.jp/) databases, with results subsequently visualized.

2.11 Mitochondrial Function Assessment

Mitochondrial membrane potential (MMP) was evaluated with the JC-1 assay kit following the manufacturer's protocol. Cells were incubated with JC-1 working solution at 37°C for 20 min, rinsed to remove residual dye, and subsequently examined by confocal microscopy for image acquisition. ATP concentrations in testicular tissue and cultured cells were quantified using an ATP assay kit. For tissue samples, 20 mg from each group was homogenized in 200 μl of lysis buffer; for cell samples, 200 μl of lysis buffer was applied per well of a six-well plate. The resulting homogenates or lysates were centrifuged at 12,000 g for 15 min at 4°C, and 20 μl of the supernatant was transferred to a 96-well plate

containing 100 µl of ATP assay working solution. Chemiluminescence analyzer readings were obtained as RLU values.

2.12 Cell Immunofluorescence Staining

Cells were seeded into confocal microplates at a density of 1×10^5 cells/well and allowed to adhere before exposure to $AlCl_3$ for 24 h. Following treatment, the culture medium was removed, and cells were fixed in 4% paraformaldehyde for 30 min. Subsequent washing with PBS (three times, 5 min each) was followed by permeabilization for 15 min and another round of PBS washing under the same conditions. Blocking was performed with goat serum for 30 min, after which primary antibodies against AKAP4 and PKA (1:300) were applied and incubated overnight at 4°C. The next day, cells were washed with PBS (three times, 5 min each) and then incubated with fluorescent secondary antibodies (1:500) for 1 h at room temperature in the dark. After antibody removal, cells were again washed with PBS (three times, 5 min each). Anti-fade mounting medium containing DAPI was subsequently added, and confocal imaging was performed 10 min later.

2.13 Determination of cyclic Adenosine Monophosphate (cAMP)

Serum or cell-lysate supernatants (normalized to identical protein concentrations) were assayed for cAMP with a commercial mouse cAMP ELISA kit (Jianglai Bio, China) following the manufacturer's instructions. In brief, 50 µL of sample was incubated with 50 µL biotinylated antibody working solution at 37°C for 60 min. After three washes, 100 µL HRP-conjugate working solution was added and the plate was incubated at 37°C for 30 min. Following five additional washes, 90 µL substrate working solution was added and the plate was kept in the dark at 37°C for 15 min. The reaction was terminated with 50 µL stop solution and the optical density was immediately read at 450 nm.

2.14 TUNEL Staining

Paraffin-embedded tissue sections were dewaxed, rehydrated.Subsequently, 100 µl of TdT Equilibration Buffer was applied and samples were equilibrated for 20 min at 37°C in a humidified chamber. After discarding the buffer, 50 µl of labeling working solution was added and cells were incubated in darkness at 37°C for 60 min. Following three washes with PBS (5 min each), anti-fade mounting medium containing DAPI was applied, and confocal images were obtained 15 min later.

2.15 Western Blotting

Mouse testicular tissue (50 mg) or cells from each well of a six-well plate were homogenized on ice with 0.5 ml lysis buffer containing protease inhibitors. Lysates were centrifuged at 12,000 rpm for 10 min at 4°C, and the resulting supernatant was collected. Protein concentration was quantified with a BCA kit (Beyotime, Shanghai, China) and normalized across samples. Equal volumes of loading buffer were added, and the mixtures were heated in a 100°C water bath for 15 min to ensure denaturation, followed by storage at − 20°C. Proteins were separated on 10% SDS-PAGE gels. Electrophoresis was initiated at 80 V and increased to 120 V once bromophenol blue reached the interface between spacer and

separation gels, continuing until the dye front reached the bottom. Transfer to membranes was performed in pre-cooled electroporation buffer at a constant current of 250 mA. Membranes were blocked with 5% blocking solution and incubated overnight at 4°C with primary antibodies against PKA(1:1000), Bcl-2(1:1000), Bax(1:1000), Cyt-C(1:1000), and BAD (1:1000), AKAP4(1:500), p-BADSer155(1:500), and cleaved caspase-3 (1:500), with GAPDH (1:5000) serving as the internal reference. After washing the next day, membranes were incubated with secondary antibodies for 1 h at room temperature. Chemiluminescent reagent was prepared at a 1:1 ratio of Solution A to Solution B, and protein bands were visualized, scanned, and quantified by grayscale analysis using ImageJ software.

2.16 Statistical Analysis

Data analysis was conducted with SPSS 24.0. Normality and variance homogeneity were first assessed. For comparisons between two groups, the Student's t-test was applied when assumptions of normal distribution and homogeneity were satisfied, whereas the t'-test was adopted otherwise. Multiple-group comparisons were evaluated by one-way ANOVA. Post hoc analyses employed the SNK test under homogeneous variance and the Games-Howell test under heterogeneous variance. Statistical significance was defined as $p < 0.05$. Results are expressed as mean ± standard deviation ($\bar{x} \pm s$). Graphs were generated using GraphPad Prism 10.5.

3 Results

3.1 $AlCl_3$ Exposure Induced Al Deposition and Pathological Injury in Mouse Testicular Tissue

Figure 1b demonstrates a marked elevation of Al content in testes following $AlCl_3$ exposure compared with controls. As shown in Fig. 1c, testicular weight declined significantly in a dose-dependent pattern. Histological analysis by HE staining revealed distinct pathological alterations, including disorganized and reduced seminiferous tubules, basement membrane disruption, a marked reduction in spermatogenic cells per tubule, nuclear pyknosis, and lymphocytic infiltration in the interstitium. The most severe alterations occurred in the high-dose exposure group (Fig. 1d).

3.2 $AlCl_3$ Exposure Reduced Sex Hormone Levels and Impaired Spermatogenesis in Mice

Figures 1e–f illustrated that epididymal sperm evaluation revealed a significant reduction in sperm concentration and PR sperm percentage, accompanied by increased proportions of NP and IM sperm. In parallel, Figs. 1g–i indicates that ELISA analysis detected significant dose-dependent reductions in serum T, LH, and FSH following $AlCl_3$ treatment compared with controls. These alterations were particularly evident in the medium- and high-dose groups ($p < 0.05$).

3.3 $AlCl_3$ Exposure Reduced AKAP4 Protein Expression and Suppressed cAMP/PKA Pathway Activity in Mice

Western blot analysis (Figs. 2a-e) demonstrated a marked reduction of AKAP4 protein expression in testicular tissue following $AlCl_3$ exposure. Parallel to this decline, PKA activity, representing a central component of the cAMP/PKA pathway, was significantly diminished. Phosphorylation of BAD at Ser155 (p-BADser155), a direct substrate of PKA, was also substantially decreased, whereas the total BAD protein level exhibited an increasing trend, most evident in the high-dose $AlCl_3$ group ($p < 0.01$). ELISA analyses revealed a significant, dose-dependent elevation of intracellular cAMP in response to $AlCl_3$ treatment ($p < 0.01$). Immunohistochemistry revealed a dose-dependent reduction in AKAP4, and PKA expression within testicular tissue (Figs. 2f-h), aligning with Western blot observations and confirming the inhibitory impact of $AlCl_3$ on the cAMP/PKA signaling pathway.

3.4 $AlCl_3$ Exposure Induced Mitochondrial Apoptosis in Mouse Testes

To assess the impact of $AlCl_3$ on testicular mitochondrial function, ATP levels were quantified in testicular tissues across treatment groups. As illustrated in Fig. 2m, ATP production declined markedly in a dose-dependent manner following $AlCl_3$ exposure, indicating mitochondrial dysfunction. Western blot analysis of apoptosis-associated proteins revealed significant upregulation of Bax and Cyt-C, together with a notable reduction in Bcl-2 expression, in the testes of $AlCl_3$-exposed mice (Figs. 2i-k). In parallel, the level of cleaved caspase-3 increased significantly (Fig. 2l), confirming activation of the mitochondrial apoptotic pathway. TUNEL staining further demonstrated a dose-dependent elevation in apoptotic cell numbers within testicular tissue (Figs. 3n-o). Collectively, these data establish that $AlCl_3$ exposure disrupts mitochondrial function and activates apoptosis in mouse testes.

3.5 Transcriptomic Analysis of GC-2spd Cells After $AlCl_3$ Exposure Revealed Enrichment of the cAMP/PKA Signaling Pathway

Assessment of GC-2spd cell viability following Al exposure demonstrated a dose-dependent decline. The half-maximal effect concentration (IC_{50}) of $AlCl_3$ was determined to be 6.604 mM. At 2 mM, viability remained above 70%, whereas exposure to 12 mM reduced viability to approximately 15% (Fig. 3b). On this basis, 2 mM was selected for subsequent experiments to maintain cellular responsiveness while minimizing extensive cytotoxicity. Transcriptomic profiling of control and 2 mM $AlCl_3$-treated cells identified 905 DEGs (Figs. 3c). GO analysis (Fig. 3d) indicated enrichment in biological processes such as second messenger–mediated signaling (GO:0019932), negative regulation of cAMP-mediated signaling (GO:0043951), regulation of ATP metabolism (GO:1903578), protein phosphatase 1 complex (GO:0000164), and ATPase-coupled transmembrane transporter activity (GO:0042626). KEGG pathway analysis (Fig. 3e) further demonstrated significant enrichment of the cAMP/PKA signaling pathway.

3.6 $AlCl_3$ Downregulated cAMP/PKA Signaling in GC-2spd Cells

As illustrated in Figs. 4a-g, Immunofluorescence staining was employed to examine the influence of $AlCl_3$ on cAMP/PKA signaling in GC-2spd cells. Exposure to 2 mM $AlCl_3$ markedly diminished the fluorescence intensities of AKAP4 and PKA, reflecting suppressed protein expression in parallel with reduced cell viability. Western blot analysis corroborated these observations. In addition, p-BADser155 was markedly attenuated, whereas total BAD protein levels increased. ELISA analysis revealed that intracellular cAMP levels were significantly elevated in GC-2spd cells exposed to 2 mM $AlCl_3$ compared with control conditions. These results indicate that the decline in GC-2spd cell viability induced by $AlCl_3$ is associated with inhibition of the cAMP/PKA signaling pathway.

3.7 $AlCl_3$ Induced Mitochondrial Apoptosis in GC-2spd Cells

As illustrated in Figs. 4h-n, MMP assays demonstrated a marked reduction in GC-2spd cells following $AlCl_3$ exposure, reflecting impaired mitochondrial function. ATP measurements further substantiated this dysfunction, as cellular ATP content was significantly reduced in the exposed group. To assess activation of the mitochondrial apoptotic pathway, Western blot analysis was performed for apoptosis-associated proteins. $AlCl_3$ treatment resulted in upregulation of Bax and Cyt-C, accompanied by a marked decrease in Bcl-2 expression. In addition, cleaved caspase-3 expression was strongly elevated, confirming activation of the mitochondrial apoptosis pathway. Collectively, the evidence demonstrates that $AlCl_3$ disrupts mitochondrial function and induces apoptosis in GC-2spd cells through the mitochondrial pathway.

3.8 AKAP4 Overexpression Reversed $AlCl_3$-Induced Decrease in cAMP/PKA Signaling Pathway Activity in GC-2spd Cells

An AKAP4-overexpressing GC-2spd cell line was generated to examine the involvement of AKAP4 in $AlCl_3$-induced cytotoxicity. As illustrated in Figs. 5a-g, in cells exposed to 2 mM $AlCl_3$, AKAP4 overexpression markedly improved survival relative to $AlCl_3$ treatment alone. Western blot analysis demonstrated increased expression of PKA, elevated p-BADser155 activity, and reduced total BAD protein levels following AKAP4 overexpression. Moreover, ELISA results demonstrated that AKAP4 overexpression fully restored intracellular cAMP levels to baseline. These data indicate that AKAP4 overexpression restored cAMP/PKA signaling activity suppressed by $AlCl_3$ and attenuated cytotoxic effects. Immunofluorescence analysis further revealed enhanced localization and expression of AKAP4 and PKA, corroborating the Western blot results and reinforcing the regulatory function of AKAP4 overexpression in sustaining cAMP/PKA signaling activity.

3.9 AKAP4 Overexpression Attenuated $AlCl_3$-Induced Mitochondrial Apoptosis in GC-2spd Cells

As illustrated in Figs. 5h-n, CCK8 assays demonstrated that 24 h exposure to 2 mM $AlCl_3$ markedly reduced cell viability, whereas AKAP4 overexpression significantly improved survival, indicating enhanced resistance to $AlCl_3$ toxicity. Mitochondrial assessment further revealed that membrane potential and ATP content were significantly elevated in cells with AKAP4 overexpression under $AlCl_3$ treatment compared with those exposed to $AlCl_3$ alone, reflecting restoration of mitochondrial function. Western blot analysis showed that $AlCl_3$-exposed GC-2spd cells with AKAP4 overexpression exhibited reduced Bax and Cyt-C expression, increased Bcl-2 expression, and diminished levels of Cleaved Caspase-3, collectively indicating suppression of mitochondrial apoptotic signaling.

4 Discussion

Rapid industrialization has led to extensive application of Al in industry, medicine, and food processing owing to its favorable physicochemical properties. Despite its utility, Al contamination has emerged as a potential threat to biological health. As a non-essential trace element, Al exhibits a prolonged half-life in the human body, and chronic intake results in accumulation with toxic consequences[29]. Evidence indicates that Al disrupts the blood-testis barrier and deposits within testicular tissue; maternal exposure during gestation can also induce Al deposition in the testes of offspring, impairing reproductive system development[30]. In the present study, Al exposure produced a dose-dependent elevation of testicular Al levels, accompanied by pathological alterations in testicular tissue and reduced numbers of mature sperm. Parallel reductions in serum T, LH, and FSH were observed, corresponding to the extent of testicular damage. According to WHO criteria, sperm motility is categorized into PR, NP, and IM, with normal thresholds defined as PR ≥ 32% or PR + NP ≥ 40%. Increasing Al exposure was associated with a progressive decline in PR sperm proportion, together with rising proportions of NP and IM sperm, the latter showing the most significant increase in the high-dose group. Assessment of testicular ATP further demonstrated reductions that paralleled declines in sperm count and motility, indicating that Al-induced reproductive toxicity in mice is closely linked to mitochondrial dysfunction.

Previous research has demonstrated a complex association between mitochondrial dysfunction and male infertility. As the primary site of cellular energy production, mitochondria are indispensable for sustaining spermatogenesis, sperm motility, and fertilization[20]. Clinically, male infertility is commonly characterized by abnormal sperm count and quality, with mitochondrial dysfunction recognized as a central mechanism underlying sperm defects. In a gradient Al exposure model established in GC-2spd cells, progressive increases in Al concentration caused a stepwise decline in MMP, impaired mitochondrial function, reduced ATP synthesis, and a consequent decrease in cell viability. These cellular alterations paralleled the pathological changes observed in the mouse model, reinforcing the conclusion that Al disrupts sperm development and motility through mitochondrial dysfunction. Beyond their role in energy metabolism, mitochondria regulate apoptosis during spermatogenesis. Decrease of

MMP triggers the opening of the mPTP, which enhances membrane permeability, promotes Cytochrome C release into the cytoplasm, initiates caspase activation, and drives apoptosis[31]. In the present study, Al exposure induced mitochondrial impairment in both mouse testes and GC-2spd cells, evidenced by diminished membrane potential, reduced ATP generation, and elevated levels of Cytochrome C and cleaved caspase-3. TUNEL staining further confirmed an increase in apoptotic bodies in Al-exposed tissues and cells. These outcomes align with observations by Xu et al. in rat liver tissue[32], indicating that Al exposure induces male reproductive toxicity by disrupting mitochondrial function and activating mitochondrial apoptotic signaling.

BAD, a pro-apoptotic member of the Bcl-2 protein family, regulates apoptosis through its phosphorylation status. The unphosphorylated form promotes apoptosis, whereas p-BAD exerts an opposing effect within the apoptotic signaling network[33]. Under apoptotic stimulation, BAD binds to anti-apoptotic proteins such as Bcl-2 and Bcl-xL via its BH3 domain, neutralizing their inhibitory control over Bax and Bak. This interaction enhances mitochondrial outer membrane permeability, leading to the release of apoptogenic factors including cytochrome C, followed by activation of the Caspase pathway and induction of apoptosis[34]. Phosphorylation alters this function, as p-BAD binds to 14-3-3 proteins and becomes sequestered in the cytoplasm, thereby preventing interaction with Bcl-2 or Bcl-xL and abolishing its pro-apoptotic activity. Through this mechanism, p-BAD contributes to cell survival signaling[35]. BAD phosphorylation is primarily mediated by serine/threonine kinases, among which PKA acts as a key regulator[36]. Binding of extracellular signaling molecules, including hormones and neurotransmitters, to membrane receptors activates G proteins, which subsequently regulate adenylate cyclase (AC) and promote ATP conversion to cAMP. Elevated cAMP activates PKA by releasing its catalytic subunit, enabling phosphorylation of BAD at Ser155 and thereby suppressing mitochondrial apoptosis[37, 38]. The efficiency and specificity of this pathway are tightly controlled by AKAPs, which bind PKA to defined subcellular compartments, ensuring rapid responsiveness to cAMP signals and precise regulation of downstream phosphorylation events [21]. Intriguingly, phosphodiesterase-4 (PDE4)—the enzyme that specifically hydrolyses cAMP—is itself activated by PKA-mediated phosphorylation. When PKA activity declines, PDE4-mediated degradation is attenuated, prolonging cAMP half-life and raising its intracellular concentration. Our data corroborate this paradigm, showing elevated cAMP levels upon PKA inhibition. Proteolysis of AKAP scaffolds localized upstream of mitochondria has been reported to attenuate mitochondrial cAMP/PKA signaling, leading to enhanced apoptosis[37]. Among AKAP family members, AKAP4 is a predominant component of the sperm fibrous sheath and plays an indispensable role in spermatogenesis, as knockout models display impaired PR in murine sperm[39, 40]. In the present study, Al exposure markedly reduced AKAP4 expression in both mouse testes and GC-2spd cells, accompanied by suppression of cAMP/PKA signaling and decreased BAD phosphorylation. These alterations disrupted the Bcl-2/Bax equilibrium, triggered mitochondrial dysfunction, and culminated in spermatogenic cell apoptosis. Transcriptomic analysis further revealed enrichment of DEGs in GO categories such as negative regulation of cAMP-mediated signaling (GO:0043951), regulation of ATP metabolism (GO:1903578), and protein phosphatase 1 complex (GO:0000164). KEGG

enrichment analysis also identified the cAMP/PKA signaling pathway, supporting the reliability of these experimental observations.

Moreover, to validate the protective function of AKAP4 against Al-induced mitochondrial apoptosis, a GC-2spd cell model with AKAP4 overexpression was generated. Transfection with the AKAP4 overexpression plasmid markedly elevated AKAP4 protein levels. Compared with non-transfected cells, AKAP4-overexpressing cells exhibited a smaller decline in MMP after Al exposure, maintained higher ATP production, and showed less inhibition of viability. In parallel, phosphorylation of BAD remained elevated and apoptosis rates were significantly reduced. These results demonstrate that AKAP4 overexpression reverses Al-induced mitochondrial apoptotic responses, consistent with observations that enhanced AKAP1 expression restores energy metabolism and neuronal survival in PD models[41]. Overall, the study identifies a mechanistic pathway through which Al disrupts spermatogenesis and motility by impairing mitochondrial function, while also establishing AKAP4 as a key regulator in resistance to Al-induced mitochondrial apoptosis, thereby providing mechanistic evidence for male reproductive toxicity.

5 Conclusion

In conclusion, this study elucidates Al-induced male reproductive toxicity and its underlying mechanism. Our findings demonstrate that Al exposure leads to testicular Al accumulation, reduced sex hormone levels, impaired spermatogenesis, and diminished sperm motility. These toxic effects are linked to mitochondrial dysfunction, characterized by decreased MMP, reduced ATP synthesis, and the activation of the mitochondrial apoptotic pathway. AKAP4, a member of the AKAP family, plays a pivotal role; its downregulation suppresses cAMP/PKA signaling, contributing to mitochondrial impairment. Importantly, AKAP4 overexpression reverses Al-induced apoptosis, offering a promising therapeutic strategy for mitigating Al-related reproductive damage.

Declarations

6 Ethics approval

This study was performed in line with the principles of the *Declaration of Helsinki*. Approval was granted by the Ethics Committee of Youjiang Medical University for Nationalities (2023091203).

7 Statement of Competing Interests

We have no known competing financial interests or personal relationships that might affect the work reported in this article.

8 Data availability

Data will be made available on reques.

9 Funding

This work was supported by the Central Guided Local Development Fund Special Project(ZY23055039), the Natural Science Foundation of Guangxi Province(2025GXNSFHA069061) and 2025 Innovation Projects of Youjiang Medical University for Nationalities Graduate Education (YXCXJH2025005, YXCXJH20250020 and YXCXJH20250027).

10 CRediT authorship contribution statement

Hongfei Hu: Writing – original draft, Validation, Methodology, Data curation, Conceptualization. **Guangji Wei**: Writing – review & editing, Writing – original draft, Validation, Methodology, Conceptualization. **Hai Lan**: Writing – review & editing, Writing – original draft, Validation, Methodology, Conceptualization. **Ningsiwei Chen:** Writing – review & editing, Writing – original draft, Validation, Methodology, Conceptualization. **Yang Feng**: Writing – review & editing. **Huixin Peng**: Writing – review & editing. **Zhenying Yang: Writing** – review & editing. **Shihua Luo**: Writing – review & editing. **Yanxin Huang**: Writing – review & editing. **Wencheng Chen**: Writing – review & editing, Resources, Supervision, Funding acquisition, Conceptualization.

References

1. Wei H, Li D, Luo Y, et al (2023) Aluminum exposure induces nephrotoxicity via fibrosis and apoptosis through the TGF-β1/Smads pathway in vivo and in vitro. Ecotoxicology and Environmental Safety 249:114422. https://doi.org/10.1016/j.ecoenv.2022.114422
2. Li B, Zhang X, Huo S, et al (2022) Aluminum activates NLRP3 inflammasome-mediated pyroptosis via reactive oxygen species to induce liver injury in mice
3. Ljunggren KG, Lidums V, Sjögren B (1991) Blood and urine concentrations of aluminium among workers exposed to aluminium flake powders. Br J Ind Med 48:106–109. https://doi.org/10.1136/oem.48.2.106
4. Priest ND, Newton D, Day JP, et al (1995) Human metabolism of aluminium-26 and gallium-67 injected as citrates. Hum Exp Toxicol 14:287–293. https://doi.org/10.1177/096032719501400309
5. M A, Av S, A S, et al (2024) Epigenetic Mechanisms of Aluminum-Induced Neurotoxicity and Alzheimer's Disease: A Focus on Non-Coding RNAs. Neurochemical research 49:. https://doi.org/10.1007/s11064-024-04214-9
6. Rodríguez J, Mandalunis PM (2018) A Review of Metal Exposure and Its Effects on Bone Health. J Toxicol 2018:4854152. https://doi.org/10.1155/2018/4854152
7. Tinkov AA, Skalny AV, Domingo JL, et al (2024) A review of the epidemiological and laboratory evidence of the role of aluminum exposure in pathogenesis of cardiovascular diseases. Environ Res 242:117740. https://doi.org/10.1016/j.envres.2023.117740
8. Hao W, Hao C, Wu C, et al (2022) Aluminum induced intestinal dysfunction via mechanical, immune, chemical and biological barriers. Chemosphere 288:132556.

https://doi.org/10.1016/j.chemosphere.2021.132556

9. Guangji W, Huixin P, Hongfei H, et al (2025) Aluminum exposure induces ferroptosis in spermatogenic cells of mice through iron overload and lipid peroxidation. Free Radical Biology and Medicine 241:789–806. https://doi.org/10.1016/j.freeradbiomed.2025.09.043
10. Huixin P, Guangji W, Yanxin H, et al (2023) Transcriptome-based analysis of the toxic effects of aluminum chloride exposure on spermatocytes. Toxicology in Vitro 92:105658. https://doi.org/10.1016/j.tiv.2023.105658
11. Peng H-X, Chai F, Chen K-H, et al (2024) Reactive Oxygen Species-Mediated Mitophagy and Cell Apoptosis are Involved in the Toxicity of Aluminum Chloride Exposure in GC-2spd. Biol Trace Elem Res 202:2616–2629. https://doi.org/10.1007/s12011-023-03848-0
12. Agarwal A, Baskaran S, Parekh N, et al (2021) Male infertility. Lancet 397:319–333. https://doi.org/10.1016/S0140-6736(20)32667-2
13. Carson SA, Kallen AN (2021) Diagnosis and Management of Infertility: A Review. JAMA 326:65–76. https://doi.org/10.1001/jama.2021.4788
14. Zhao Q, Fang Z, Wang P, et al (2025) Polylactic Acid Micro/Nanoplastic Exposure Induces Male Reproductive Toxicity by Disrupting Spermatogenesis and Mitochondrial Dysfunction in Mice. ACS Nano 19:5589–5603. https://doi.org/10.1021/acsnano.4c15112
15. Jamalan M, Ghaffari MA, Hoseinzadeh P, et al (2016) Human Sperm Quality and Metal Toxicants: Protective Effects of some Flavonoids on Male Reproductive Function. Int J Fertil Steril 10:215–223. https://doi.org/10.22074/ijfs.2016.4912
16. Klein JP, Mold M, Mery L, et al (2014) Aluminum content of human semen: implications for semen quality. Reprod Toxicol 50:43–48. https://doi.org/10.1016/j.reprotox.2014.10.001
17. Martinez CS, Escobar AG, Uranga-Ocio JA, et al (2017) Aluminum exposure for 60 days at human dietary levels impairs spermatogenesis and sperm quality in rats. Reproductive Toxicology 73:128–141. https://doi.org/10.1016/j.reprotox.2017.08.008
18. Miska-Schramm A, Kapusta J, Kruczek M (2017) The Effect of Aluminum Exposure on Reproductive Ability in the Bank Vole (Myodes glareolus). Biol Trace Elem Res 177:97–106. https://doi.org/10.1007/s12011-016-0848-3
19. Yousef MI, El-Morsy AMA, Hassan MS (2005) Aluminium-induced deterioration in reproductive performance and seminal plasma biochemistry of male rabbits: Protective role of ascorbic acid. Toxicology 215:97–107. https://doi.org/10.1016/j.tox.2005.06.025
20. Mai Z, Yang D, Wang D, et al (2024) A narrative review of mitochondrial dysfunction and male infertility. Transl Androl Urol 13:2134–2145. https://doi.org/10.21037/tau-24-262
21. Baro Graf C, Ritagliati C, Stival C, et al (2020) Everything you ever wanted to know about PKA regulation and its involvement in mammalian sperm capacitation. Molecular and Cellular Endocrinology 518:110992. https://doi.org/10.1016/j.mce.2020.110992
22. Akabane S, Oka T (2024) Insights into the regulation of mitochondrial functions by protein kinase A-mediated phosphorylation. The Journal of Biochemistry 175:1–7.

https://doi.org/10.1093/jb/mvad075

23. Wang X, Chen S, Wan J, et al (2025) Iloprost Concentration-Dependently Attenuates Platelet Function and Apoptosis by Elevating PKA Activity. J Cell Mol Med 29:e70403. https://doi.org/10.1111/jcmm.70403
24. Hu Y, Yu H, Pask AJ, et al (2009) A-kinase anchoring protein 4 has a conserved role in mammalian spermatogenesis. Reproduction 137:645–653. https://doi.org/10.1530/REP-08-0337
25. Zhang Q, Zhang X, Yang B, et al (2024) Ligustilide-loaded liposome ameliorates mitochondrial impairments and improves cognitive function via the PKA/AKAP1 signaling pathway in a mouse model of Alzheimer's disease. CNS Neurosci Ther 30:e14460. https://doi.org/10.1111/cns.14460
26. Liang C, He Y, Liu Y, et al (2020) Fluoride exposure alters the ultra-structure of sperm flagellum via reducing key protein expressions in testis. Chemosphere 246:125772. https://doi.org/10.1016/j.chemosphere.2019.125772
27. Peng H, Huang Y, Wei G, et al (2024) Testicular Toxicity in Rats Exposed to AlCl3: a Proteomics Study. Biol Trace Elem Res 202:1084–1102. https://doi.org/10.1007/s12011-023-03745-6
28. Hu H, Wei G, Lan H, et al (2025) Oxidative stress and iron homeostasis imbalance mediate AlCl3-induced liver damage in mice. Journal of Environmental Sciences. https://doi.org/10.1016/j.jes.2025.04.055
29. Yokel RA (2020) Aluminum reproductive toxicity: a summary and interpretation of scientific reports. Crit Rev Toxicol 50:551–593. https://doi.org/10.1080/10408444.2020.1801575
30. Chen J, Xia Y, Ben Y, et al (2024) Embryonic exposure to aluminum chloride blocks the onset of spermatogenesis through disturbing the dynamics of testicular tight junctions via upregulating Slc25a5 in offspring. Science of The Total Environment 915:170128. https://doi.org/10.1016/j.scitotenv.2024.170128
31. Meng K, Liu Q, Qin Y, et al (2025) Mechanism of mitochondrial oxidative phosphorylation disorder in male infertility. Chin Med J (Engl) 138:379–388. https://doi.org/10.1097/CM9.0000000000003126
32. Xu F, Liu Y, Zhao H, et al (2017) Aluminum chloride caused liver dysfunction and mitochondrial energy metabolism disorder in rat. J Inorg Biochem 174:55–62. https://doi.org/10.1016/j.jinorgbio.2017.04.016
33. Pitchaimani V, Arumugam S, Thandavarayan RA, et al (2014) Fasting mediated increase in p-BADser155 and p-AKTser473 in the prefrontal cortex of mice. Neuroscience Letters 579:134–139. https://doi.org/10.1016/j.neulet.2014.07.009
34. Kuo C-T, Hsu M-J, Chen B-C, et al (2008) Denbinobin induces apoptosis in human lung adenocarcinoma cells via Akt inactivation, Bad activation, and mitochondrial dysfunction. Toxicol Lett 177:48–58. https://doi.org/10.1016/j.toxlet.2007.12.009
35. Jiao L, Yi W, Chang Y-R, et al (2024) Inhibition of P21-activated Kinase 1 Promotes Vascular Smooth Muscle Cells Apoptosis Through Reduction of Phosphorylation of Bad. Am J Hypertens 37:46–52. https://doi.org/10.1093/ajh/hpad007

36. Harada H, Becknell B, Wilm M, et al (1999) Phosphorylation and inactivation of BAD by mitochondria-anchored protein kinase A. Mol Cell 3:413–422. https://doi.org/10.1016/s1097-2765(00)80469-4
37. Ould Amer Y, Hebert-Chatelain E (2018) Mitochondrial cAMP-PKA signaling: What do we really know? Biochim Biophys Acta Bioenerg 1859:868–877. https://doi.org/10.1016/j.bbabio.2018.04.005
38. Affaitati A, Cardone L, de Cristofaro T, et al (2003) Essential role of A-kinase anchor protein 121 for cAMP signaling to mitochondria. J Biol Chem 278:4286–4294. https://doi.org/10.1074/jbc.M209941200
39. Moretti E, Scapigliati G, Pascarelli NA, et al (2007) Localization of AKAP4 and tubulin proteins in sperm with reduced motility. Asian J Androl 9:641–649. https://doi.org/10.1111/j.1745-7262.2007.00267.x
40. Miki K, Willis WD, Brown PR, et al (2002) Targeted disruption of the Akap4 gene causes defects in sperm flagellum and motility. Dev Biol 248:331–342. https://doi.org/10.1006/dbio.2002.0728
41. Scorziello A, Borzacchiello D, Sisalli MJ, et al (2020) Mitochondrial Homeostasis and Signaling in Parkinson's Disease. Front Aging Neurosci 12:100. https://doi.org/10.3389/fnagi.2020.00100

Figures

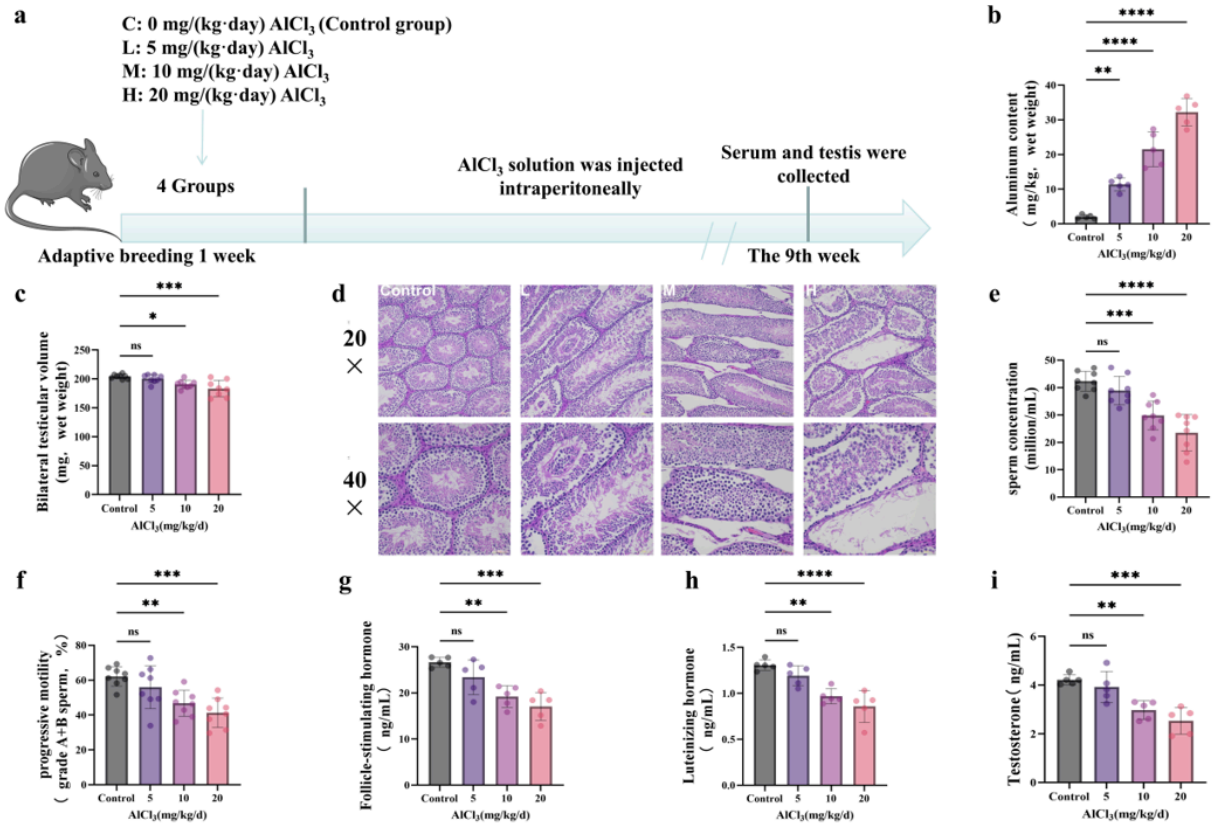


Figure 1

$AlCl_3$ exposure disrupts male reproductive function in mice. (a) Experimental timeline. (b) Testicular aluminum accumulation. (c) Bilateral testis weight. (d) Representative H&E-stained sections. (e) Sperm count. (f) Progressive motility percentage. (g–i) Serum FSH, LH and testosterone. * denotes significant differences (*P < 0.05, **P < 0.01, ***P < 0.001, ****P < 0.0001).

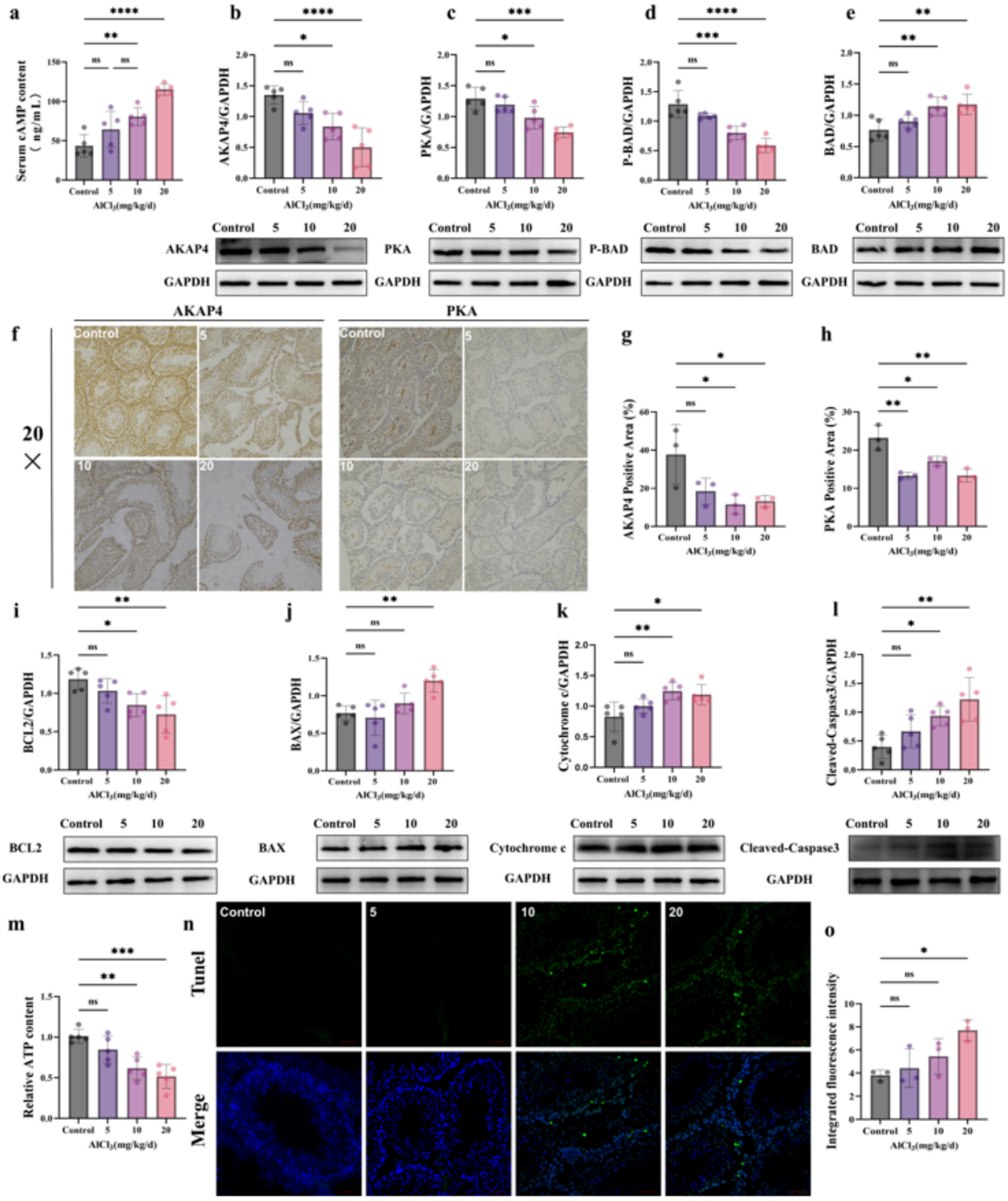


Figure 2

$AlCl_3$ inhibits testicular cAMP/PKA signaling and triggers testicular mitochondrial apoptosis. (a) Serum cAMP. (b–e) AKAP4, PKA, P-BAD and BAD protein levels. (f-h) AKAP4 and PKA IHC with quantification. (i–l) BCL2, BAX, cytochrome c and cleaved-caspase-3 levels. (m) ATP content of testicular tissue. (n, o) TUNEL images and apoptotic index (scale bar: 50 μm). * denotes significant differences (*P < 0.05, **P < 0.01, ***P < 0.001, ****P < 0.0001).

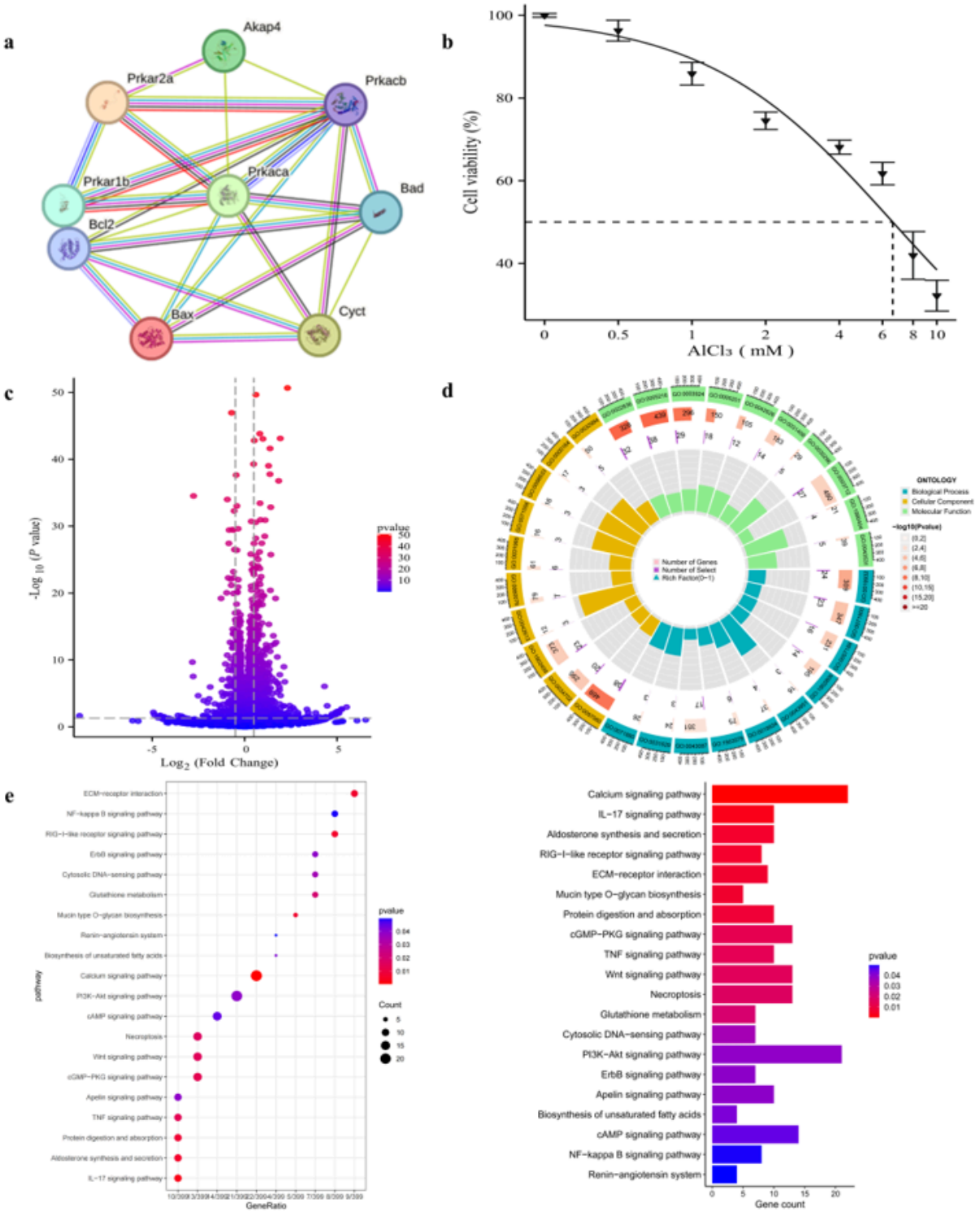


Figure 3

Transcriptomic analysis of GC-2spd cells exposed to 2 mM $AlCl_3$. (a) AKAP4–PKA subunit interaction. (b) IC_{50} curve. (c) DEG volcano plot. (d) GO analysis. (e) KEGG enrichment.

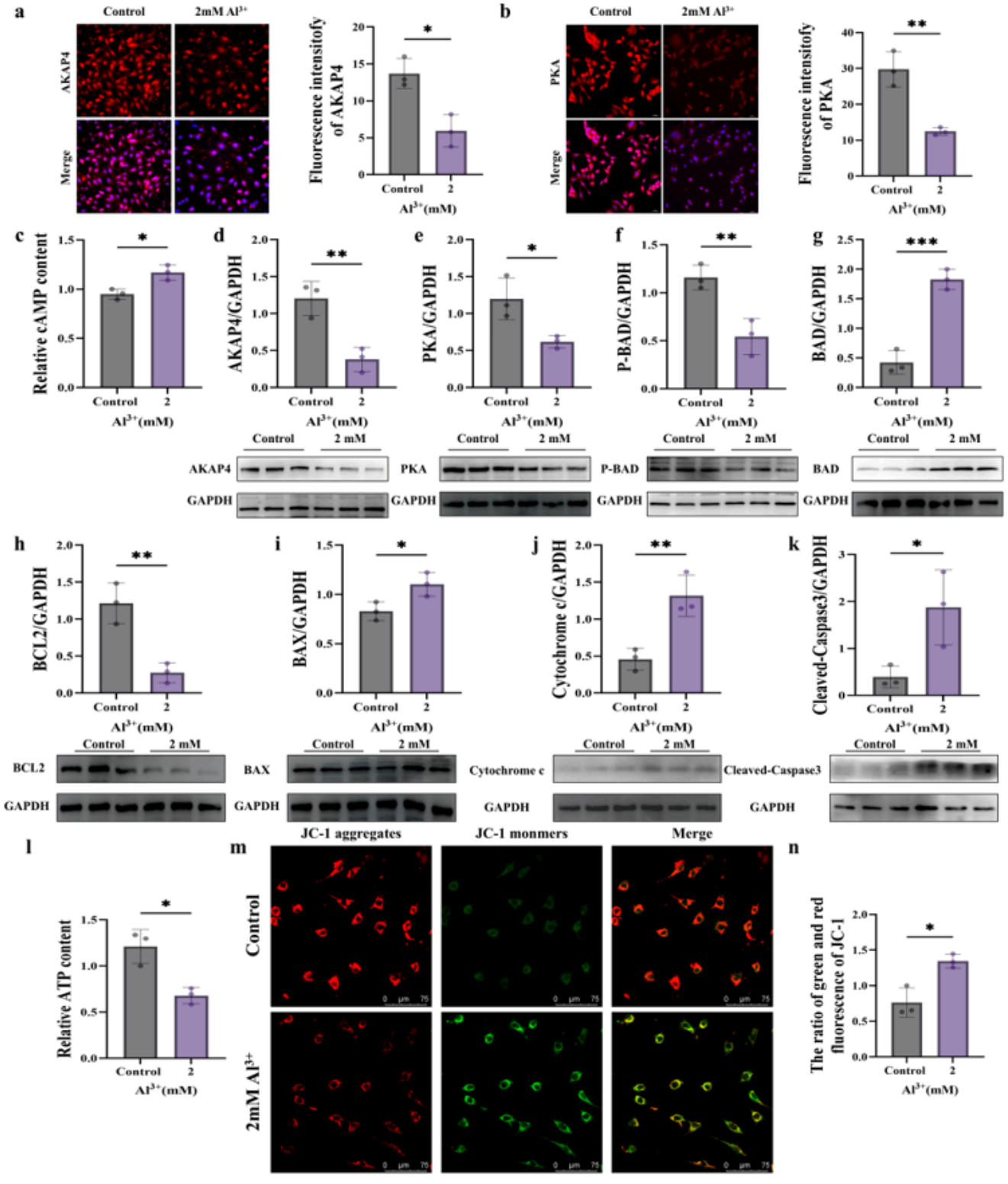


Figure 4

2 mM $AlCl_3$ suppresses cAMP/PKA signaling and induces mitochondrial apoptosis in GC-2spd cells. (a, b) AKAP4/PKA immunofluorescence (50 μm). (c) cAMP level. (d–g) Western blots of AKAP4, PKA, P-

BAD and BAD. (h–k) BCL2, BAX, cytochrome c and cleaved-caspase-3 Western blots. (l) Relative ATP content. (m, n) JC-1 images and quantification (scale bar: 75 μm). * denotes significant differences (*P < 0.05, **P < 0.01, ***P < 0.001, ****P < 0.0001).

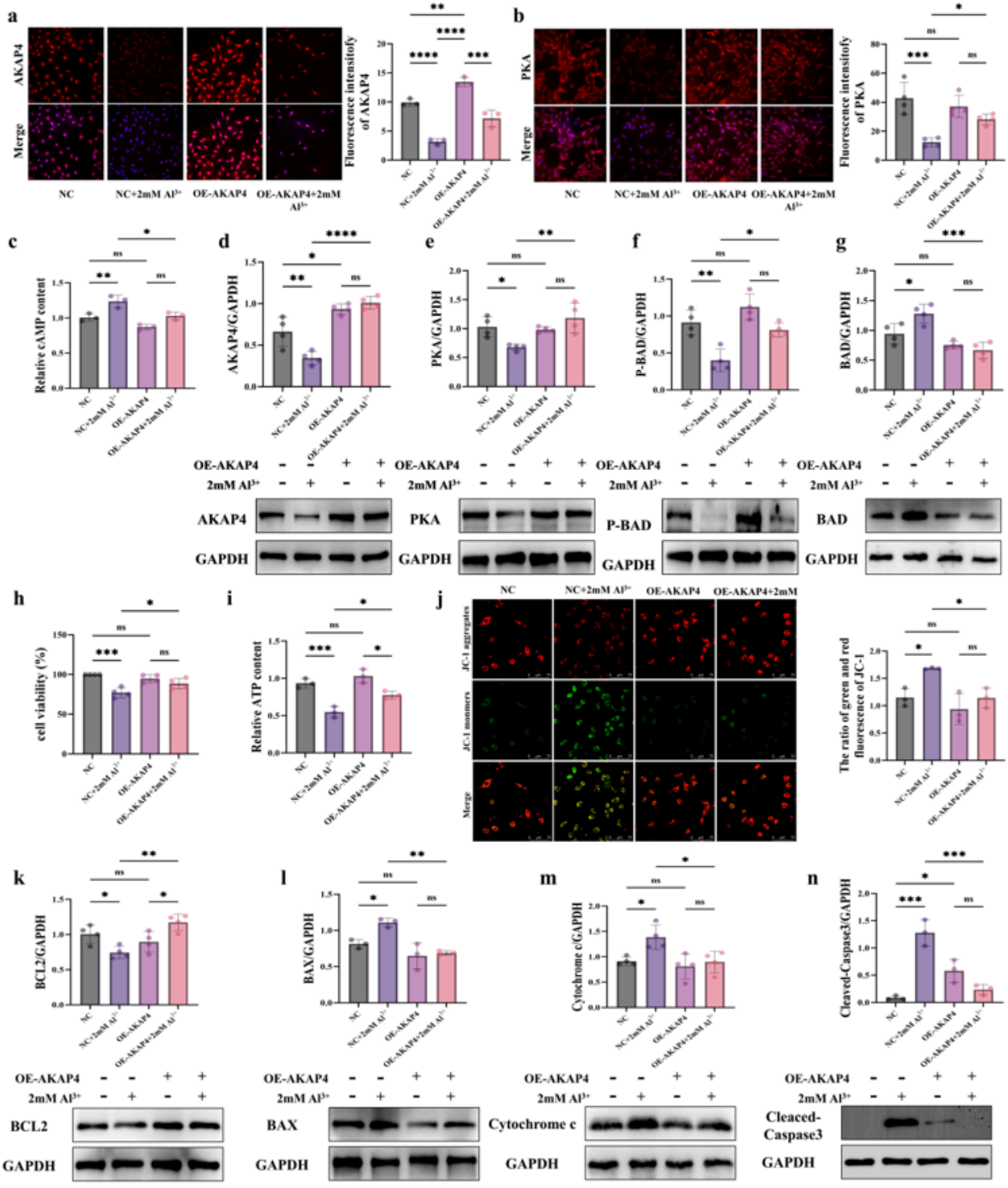


Figure 5

AKAP4 overexpression rescues $AlCl_3$-suppressed cAMP/PKA signaling and attenuates $AlCl_3$-induced mitochondrial apoptosis. (a, b) AKAP4/PKA immunofluorescence (250 μm). (c) cAMP level. (d–g)

AKAP4, PKA, P-BAD and BAD Western blots. (h) Cell viability. (i) Relative ATP content. (j) JC-1 images and quantification (75 μm). (k–n) BCL2, BAX, cytochrome c and cleaved-caspase-3 Western blots. * denotes significant differences (*P < 0.05, **P < 0.01, ***P < 0.001, ****P < 0.0001).

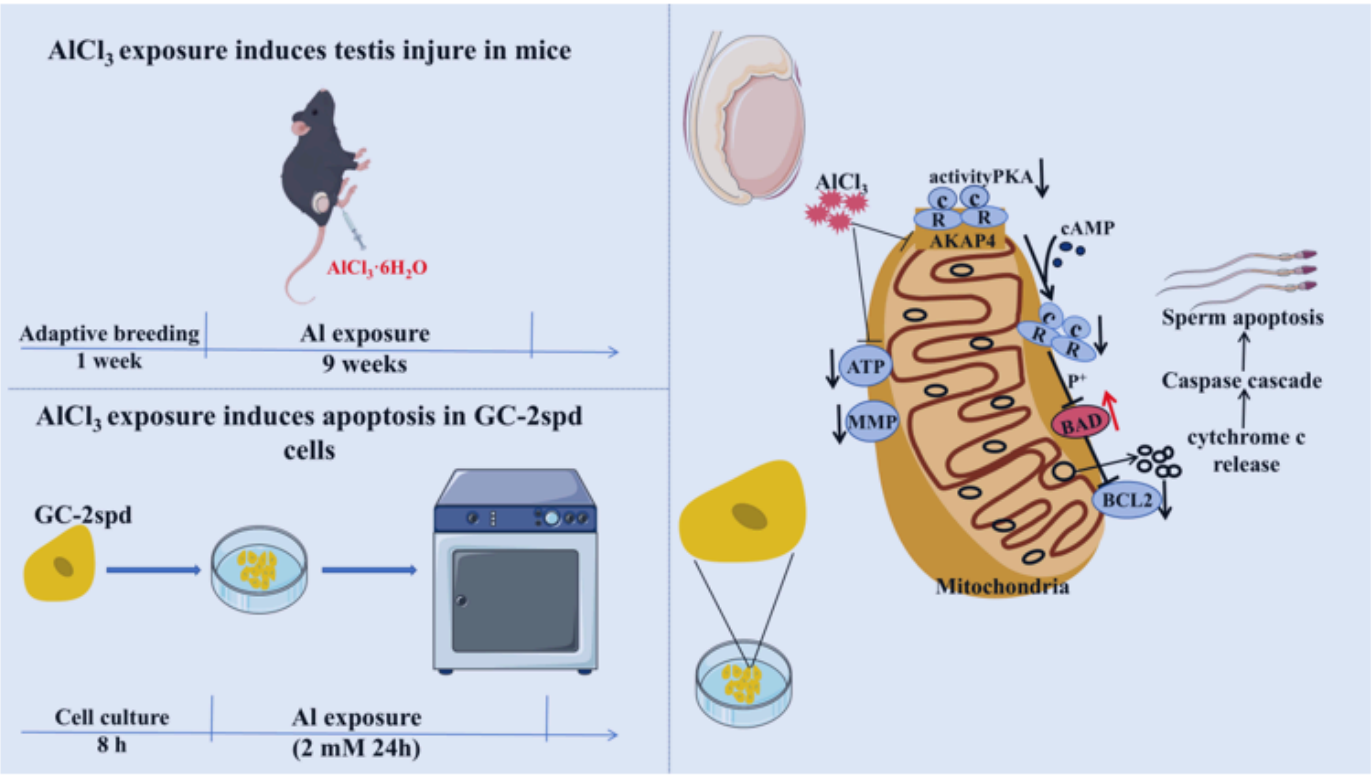


Figure 6

Figure 5. Mechanism hypothesis diagram.

Supplementary Files

This is a list of supplementary files associated with this preprint. Click to download.

- supplementaryfile.pdf